Anisotropic surface broadening and core depletion during the evolution of a strong-field induced nanoplasma

Camila Bacellar[1,2†], Adam S. Chatterley[1,2§], Florian Lackner[1,2¶], C. D. Pemmaraju[1‡], Rico Mayro P. Tanyag[3∓], Deepak Verma[3], Charles Bernando[4], Sean M. O. O'Connell[3▽], Maximilian Bucher[5], Ken R. Ferguson[6], Tais Gorkhover[6,7,8❖], Ryan N. Coffee[6], Giacomo Coslovich[6], Dipanwita Ray[6], Timur Osipov[6], Daniel M. Neumark[1,2], Christoph Bostedt[6,9†*], Andrey F. Vilesov[3,4*], and Oliver Gessner[1*]

[1] Chemical Sciences Division, Lawrence Berkeley National Laboratory, Berkeley, California 94720, USA

[2] Department of Chemistry, University of California Berkeley, Berkeley, California 94720, USA.

[3] Department of Chemistry, University of Southern California, Los Angeles, California 90089, USA

[4] Department of Physics and Astronomy, University of Southern California, Los Angeles, California 90089, USA

[5] Argonne National Laboratory, 9700 South Cass Avenue B109, Lemont, IL 60439, USA.

[6] Linac Coherent Light Source, LCLS, SLAC National Accelerator Laboratory, 2575 Sand Hill Road, Menlo Park, California 94025, USA

[7] Institute of Optics and Atomic Physics, Technical University of Berlin, Hardenbergstraße 36, 10623 Berlin, Germany

[8] Stanford PULSE Institute, SLAC National Accelerator Laboratory, 2575 Sand Hill Road, Menlo Park, California 94025, USA

[9] Department of Physics and Astronomy, Northwestern University, 2145 Sheridan Road, Evanston, IL 60208, USA.

Present addresses:

† Paul Scherrer Institut, Forschungsstrasse 111, 5232 Villigen-PSI, Switzerland

§ Department of Chemistry, Aarhus University, Langelandsgade 140, 8000 Aarhus C, Denmark

¶ Institute of Experimental Physics, Graz University of Technology, Petersgasse 16, A-8010 Graz, Austria

‡ Theory Institute for Materials and Energy Spectroscopies, SLAC National Accelerator Laboratory, Menlo Park, California 94025, USA

∓ Max-Born-Institut für Nichtlineare Optik und Kurzzeitspektroskopie, Max-Born-Straße 2A, 12489 Berlin, Germany

▽ University of Miami Rosenstiel School of Marine and Atmospheric Science, Miami, Florida 33149, USA

❖ University of Hamburg, Center for Free-Electron Laser Science, Luruper Chaussee 149, 22761 Hamburg, Germany

* corresponding authors: christoph.bostedt@psi.ch, vilesov@usc.edu, ogessner@lbl.gov

Abstract

Strong-field ionization of nanoscale clusters provides excellent opportunities to study the complex correlated electronic and nuclear dynamics of near-solid density plasmas. Yet, monitoring ultrafast, nanoscopic dynamics in real-time is challenging, which often complicates a direct comparison between theory and experiment. Here, near-infrared laser-induced plasma dynamics in ~600 nm diameter helium droplets are studied by femtosecond time-resolved X-ray coherent diffractive imaging. An anisotropic, ~20 nm wide surface region, defined as the range where the density lies between 10% and 90% of the core value, is established within ~100 fs, in qualitative agreement with theoretical predictions. At longer timescales, however, the width of this region remains largely constant while the radius of the dense plasma core shrinks at average rates of ≈71 nm/ps along and ≈33 nm/ps perpendicular to the laser polarization. These dynamics are not captured by previous plasma expansion models. The observations are phenomenologically described within a numerical simulation; details of the underlying physics, however, remain to be explored.

Main Text

Studying strong-field ionization (SFI) of nanoclusters can yield a better understanding of the coupled electronic-nuclear dynamics underlying the formation and expansion of nanoplasmas. Until recently, direct real-time access to these dynamics, which typically proceed on femtosecond to picosecond temporal scales and nanometer spatial scales, was challenging. Most experiments focused on electron and ion kinetic energy and momentum distributions, which superimpose signals from all stages of the nanoplasma evolution [1-12]. The advent of X-ray free electron lasers (XFELs) has enabled a new class of single-shot X-ray coherent diffractive imaging (CDI) experiments that probe transient

plasma shapes and electron density distributions in real-time and with ≲100 fs temporal resolution [13-20]. CDI experiments by Gorkhover *et al.* demonstrated that SFI of Xe_N clusters, ~30-60 nm in diameter, with near-infrared (NIR) laser pulses at $\approx 2 \times 10^{15}$ W/cm^2 induces an isotropic increase of the surface width [14], instead of a uniform cluster expansion, as had previously been suggested [1,2]. Time-resolved wide-angle X-ray scattering (WAXS) study by Ueda and co-workers supports this picture and provides additional insight into the associated loss of crystalline order [20]. Microscopic particle-in-cell (Mic-PIC) calculations predict a similar surface broadening process in a nanoplasma generated by SFI of ~50 nm diameter hydrogen clusters [21]. In addition, the calculations yield a slightly enhanced surface width along the laser polarization axis compared to the perpendicular directions, and a small (~few percent) surface anisotropy that persists for at least the first ~100 fs of the hydrodynamic expansion [21]. Electron and ion energy and momentum distributions resulting from SFI of nano-clusters provided evidence for anisotropic nanoplasma processes [22-30]. However, monitoring the emergence and evolution of anisotropies in real-time has not yet been achieved. We use ultrafast CDI to reveal pronounced anisotropic nanoplasma dynamics that emerge within the ≈40 fs laser pulse duration and continue to evolve on picosecond timescales. The results reproduce a predicted anisotropic surface broadening process during the laser-plasma interaction [21] and reveal additional effects including a saturation of the surface width after ~100-200 fs and a pronounced anisotropic shrinking of the plasma core on timescales of up to tens of picoseconds.

A schematic of the experimental setup using the LAMP chamber of the Linac Coherent Light Source (LCLS) AMO instrument is shown in Fig. 1a [31]. Helium droplets

with an average radius $R \approx 300$ nm are generated by continuous expansion of He fluid at 20 bar through a cold (4.7 K) 5 μm wide nozzle [32]. The droplet beam is intercepted by femtosecond NIR laser pulses ($\lambda = 800$ nm, pulse width $\tau \approx 40$ fs, focal size $2w \approx 75$ μm) at intensities of $\approx 3\text{-}4\times10^{15}$ W/cm^2, leading to SFI of He atoms [33] and the formation of a nanoplasma. The temporal evolution of the plasma is monitored by recording X-ray diffraction patterns, each generated by the interaction of a single LCLS X-ray pulse ($\lambda = 2.07$ nm, $\tau \approx 100$ fs, $2w \approx 3\text{-}5$ μm) with a single droplet using NIR-pump/X-ray-probe delays from a few fs up to 100 ps. For each diffraction pattern, an ion time-of-flight (TOF) spectrum is recorded in coincidence, from which the degree of ionization and the ion kinetic energy distribution are obtained as outlined in the Supplemental Material [34].

Representative single-shot diffraction patterns corresponding to three different time delays between the NIR pump pulse and the X-ray probe pulse are shown in Fig. 1b-d. The NIR pump pulse arrives before (after) the X-ray probe pulse for positive (negative) delays. At negative and small positive delays up to ~300 fs, the vast majority of images consist of a series of concentric rings, indicating a predominantly spherical shape of helium nanodroplets [13] (Fig. 1b). At 2.1 ps delay, however, strongly elliptical patterns are observed with their long axes aligned along the NIR polarization axis (Fig. 1c). After 20 ps, only streaked images are observed with their intensities strongly concentrated along the NIR polarization axis (Fig. 1d). Note that for a nominal NIR polarization angle of +45º (clockwise), an additional offset angle of ~23º is observed between the patterns and the nominal polarization axis. The offset is ascribed to accidental polarization control in the optical beam path, as discussed in section II.C of the Supplemental Material [34]. Rotation of the NIR polarization by 90° leads to a corresponding rotation of the elliptical patterns as

demonstrated in Fig. 1e,f. We note that ~50% of the diffraction images recorded at 2.1 ps delay exhibit speckled patterns that cannot be readily analyzed. A more detailed description of the relative abundances of various patterns and the analysis of angular correlations are presented in the Supplemental Material [34].

X-ray diffraction patterns are sensitive to the density distribution of electrons. Based on calculations for SFI of hydrogen clusters [21], we assume that electron and ion density distributions become very similar within less than ~100 fs and, therefore, that the diffraction images largely reflect the distributions of both electrons and ions of quasi-neutral plasmas. The observed elliptical patterns (Fig. 1c,e,f) are modeled by diffraction from spheroids (smoothed lines) in very good agreement with the experiment [13,34]. For spheroidal shapes with a sharp surface, the scattering intensity, I, scales as $I(q,\Phi)\sim q^{-4}cos^2\left(q\cdot R_{eff}\right)$, where $q=|\vec{q}|$ is the modulus of the scattering vector, Φ is the azimuthal angle in the detector plane and R_{eff} is the Φ-dependent radius of the spheroid's projection onto the detector (see Supplemental Material) [13,34,35]. This q-dependence is readily apparent in Fig. 2a, which shows the azimuthally integrated quantity $I\cdot q^4$ obtained from a diffraction image at negative pump-probe delay, i.e., for an unperturbed spherical droplet with a sharp surface. In contrast, Fig. 2b shows the same quantity for a droplet 74 fs after interaction with the NIR pulse. In this case, the intensity drops faster than q^{-4}, and is well captured by a modified description $I(q,\Phi)\sim q^{-\alpha}cos^2\left(q\cdot R_{eff}\right)$ with $\alpha\approx 5.5$. Values of $\alpha>4$ indicate that the plasma surface is not sharp but has a finite width, ε, defined as the range over which the density drops from 90% to 10% of the value in the interior. For each droplet/nanoplasma, the width ε is obtained from the measured decay exponent α. The required ε - α relationship is derived in a two-step procedure. In the first step, a modified

Fermi function is used to model the radial droplet density distribution [15,21], and simulated diffraction patterns are calculated for a variety of droplet sizes, shapes, and surface widths. In the second step, the radial intensity distributions of the simulated patterns are fit to the description given above in relation to Fig. 2a,b, providing a unique value α and for each ε, and vice versa, as shown in Fig. S7 of the Supplemental Material [34].

Figure 2c shows the fitted decay exponents α (right) and corresponding surface widths ε (left) for scattering intensities averaged over $\Delta\Phi = 90°$ wide slices parallel (red) and perpendicular (blue) to the NIR polarization axis, for NIR–X-ray time delays -300 fs $< \Delta t <$ +300 fs. The inset shows the difference between the two curves (green). Figure 2c reveals that ε increases monotonically over a few hundred femtoseconds in both parallel and perpendicular directions. Additionally, at the peak of the NIR pulse around time zero, a difference in surface widths, $\Delta\varepsilon$, of approximately 4-5 nm is established within less than 100 fs and remains constant throughout the continued surface broadening. Beyond ~100-200 fs delay, the surface widths are saturating at values of ≈21 nm at the poles (i.e., along the laser polarization) and ≈16 nm at the equator. Similar, albeit slightly smaller surface widths are observed at 2.1 ps delay. Note that the likely appearance of a pedestal in the surface profile (see below) may lead to an underestimation of the surface width by up to ~30%. The saturation of the surface width after a few hundred femtoseconds is contrasted by a very pronounced, continuous shape change of the droplet core as evidenced by the strongly elliptical patterns at 2.1 ps (Fig. 1c,e,f) and streaks at 20 ps (Fig. 1d) pump-probe delays. The increase of the average diffraction ring spacing shows that the droplet core does not expand, as expected from previous models [1,2], but instead shrinks with increasing time delay, which has also been noted in other more recent studies [14,15,21].

Interestingly, up to ~100 fs delay, the average surface broadening rates of ~70-95 nm/ps observed here are remarkably close to the ~70 nm/ps rate predicted by Fennel and co-workers for smaller hydrogen clusters [21] (H_N, $N \approx 3\times10^6$). Additionally, the difference $\Delta\varepsilon$ between the polar and equatorial surface widths is essentially established within the NIR pulse duration and remains constant thereafter in both theory and experiment (Fig. 3b in ref. [21] and Fig. 2c). The extent of this difference is ~5 nm for the He droplets compared to ~1.4 nm in the H_N clusters. The larger polar surface width is predominantly ascribed to enhanced Coulomb explosion enabled by the oscillatory motion of the quasi-free plasma electrons in the laser field, leading to reduced, time-averaged ion screening at the poles [21,25]. The laser intensity in the He droplet experiment is up to four times higher than the one in the calculation for H_N clusters, which may lead to larger oscillation amplitudes and correspondingly stronger Coulomb repulsion effects in the droplets [36]. Thus, the observed anisotropic plasma surface dynamics up to ~100 fs qualitatively reproduce theoretical predictions. The saturation of the surface width and the pronounced core anisotropies emerging on picosecond timescales, however, are unexpected and represent key new insights revealed by this study. The calculations by Peltz *et al.* [21] do not indicate a saturation of the surface width. Note, however, that the theoretical work is restricted to timescales ≤100 fs, where saturation effects in the experimental data presented here are also very limited (Fig. 2c). Experiments by Gorkhover *et al.* also do not report any surface width saturation effects (or anisotropies) for SFI of small Xe clusters up to 500 fs [14]. However, the surface of the Xe clusters broadens significantly slower than the He droplet surface and the relatively small Xe aggregates essentially disintegrate before their surface width becomes comparable to the saturation

values of ε observed in this work. The observations described herein, therefore, do not disagree with previous results but rather extend the range of CDI studies on SFI induced nanoplasmas to previously unexplored time- and length-scales.

A particularly surprising finding is that the core size and shape evolution does not mirror the surface broadening dynamics. During the first 2.1 ps, the core radii drop at average rates of $dR_{para} / dt \approx$ -71 nm/ps and $dR_{perp} / dt \approx$ -33 nm/ps, reducing the droplet diameter from pole to pole to about 2/3 of the equatorial diameter (aspect ratio AR≈1.5). The average droplet radius is reduced by ~100 nm during this time while the surface width remains nearly constant at ~15-20 nm. We note that the average shrinking rate estimates are based on the assumption that the elliptical patterns recorded at 2.1 ps delay emerge from statistical sampling of the original, unperturbed ensemble of droplets with an average radius of ~300 nm and an average AR of 1.06 [37]. The abovementioned presence of speckled diffraction patterns at 2.1 ps delay indicates that there may be alternative plasma evolution mechanisms. Generally, such speckles are associated with highly inhomogeneous objects, such as droplets undergoing disintegration into multiple fragments. Unfortunately, the large gap between the detector plates required in this work renders a reconstruction of the corresponding density distributions via a phase retrieval algorithm, as shown in our previous works, unfeasible [18,38,39]. The streaked images recorded at a pump-probe delay of 20 ps are consistent with a continued flattening of the droplet shapes along the NIR polarization on tens of picosecond timescales. Ion TOF spectra recorded in coincidence with the diffraction patterns show that approximately twice as many ions are ejected parallel to the laser polarization (per unit solid angle) as compared to the perpendicular direction, while the total number of ejected He^+ ions is comparable to

that of the number of atoms in the droplets. These complementary measurements are consistent with a continued anisotropic ion ejection well beyond the duration of the laser-droplet interaction. Additionally, the characteristic ion kinetic energies are also higher along the laser polarization (see Supplemental Material [34]). At a pump-probe delay of 100 ps, no diffraction patterns are detected, indicating that all droplets have disintegrated before this point in time. These findings for large He nanodroplets differ from the suspended expansion observed in comparably sized Xe clusters, for which initial surface peeling is followed by very slow (~ns) dynamics within a residual, neutral plasma core [15,40,41]. We note that a nanometer-resolved evolution of the droplet core sizes, similar to that of the surface widths displayed in Fig. 2c, cannot be directly observed due to the inherent size distribution of the droplets. Changes in aspect ratios during the first 300 fs of evolution cannot be detected either. Based on the average rate of the core shrinking, a spherical droplet would acquire an aspect ratio of ~1.04 during this time, which is smaller than the average droplet aspect ratio in the beam. However, the key finding of a continued anisotropic core depletion as outlined above is supported by the data recorded at 2.1 ps and 20 ps pump-probe delays and by a statistical analysis of the size distributions for various pump-probe delays as described in section II.B of the Supplemental Material [34].

Detailed theoretical modeling of nanoplasma dynamics comparable to those for smaller hydrogen [21] and xenon [41] clusters is not available for large He nanodroplets containing ~3-5 orders of magnitude more atoms. Liseykina and Bauer [42] predicted strongly inhomogeneous, anisotropic ionization dynamics in micrometer sized He droplets exposed to NIR laser intensities of 5.2×10^{17} W/cm^2. It is possible that anisotropic ionization effects contribute to the dynamics observed here. However, the starkly different excitation

regimes make a direct comparison challenging, as described in more detail in the Supplemental Material. In the absence of a bottom-up description, we resort to a numerical mass-flow simulation to provide a self-consistent interpretation of the observed scattering patterns and TOF spectra that obeys basic laws of mass and energy conservation. A detailed description of the simulation is given in the Supplemental Material [34]. Briefly, the simulation is based on the assumption that the shape evolution is predominantly driven by ion ejection from the plasma surface, in agreement with other theoretical [21,41] and experimental [14,20,41] works. The average velocity by which an ion is moving away from the plasma center is assumed to be related to the local density and the density gradient, approaching zero effective radial velocity inside the droplet bulk and maximum radial velocity in the free atom limit. Within this picture, an instantaneous radial density profile can be translated into an effective instantaneous radial velocity profile, which in turn affects the further evolution of the density profile. Numerical propagation of the density distribution and the effective mass transport away from the droplet yields the simulation results displayed in Fig. 3. We emphasize that this simulation is mostly phenomenological and based on a set of adjustable parameters. The underlying physics, such as time-dependent charge and energy distributions and the relative contributions of hydrodynamic expansion and Coulomb explosion dynamics, remains to be explored by significantly more sophisticated calculations. The simulation does, however, provide a consistent description of all experimental data, i.e. scattering images and TOF spectra.

Figure 3a compares the average experimentally derived density profiles along (orange) and perpendicular to (light blue) the NIR polarization with the results of the simulation (red and blue shaded areas). Note that the stretched-out pedestals at large r

cannot be detected in the current experiment [34]. The free atom velocities employed for the simulations correspond to kinetic energies of 500 eV and 100 eV for parallel and perpendicular directions, respectively. These energies are chosen such that they are consistent with the differences between kinetic energy distributions measured parallel and perpendicular to the NIR polarization [34]. Figure 3b shows three-dimensional renderings of the simulated density profiles. For improved clarity, the shapes are cut in half at the indicated plane and the front half is offset. Local densities are represented by the density of points as well as the indicated color code. The simulation captures the key aspects of the observed plasma shape evolution, i.e., the saturation of surface width within hundreds of femtoseconds and the rapid, continued anisotropic shrinking of the high-density core. Anisotropies in ion emission intensities and kinetic energies from SFI induced nanoplasmas have previously been reported by a number of groups [22-29]. However, these anisotropies were recorded by time-integrated techniques that do not provide direct access to the dynamics taking place during and after the interaction of the laser field with the plasma. The study presented here closes this gap, revealing a significantly more detailed picture of the ultrafast, nanoscale dynamics underlying the final product distributions.

In summary, this work provides the first real-time measurements of the formation and evolution of an anisotropic nanoplasma. An anisotropic plasma surface appears within ~100 fs and saturates within ~300 fs after SFI with characteristic widths of ~20 nm parallel and ~15 nm perpendicular to the strong field polarization. The observed dynamics in helium nanodroplets are in qualitative agreement with related theoretical predictions for hydrogen clusters. While the surface width remains almost constant for at least 2.1 ps after SFI, the shape of the plasma core changes significantly during the same period, shrinking

by ~45% and ~19% in parallel and perpendicular directions, respectively. A numerical model reproduces the observed trends, the underlying physics, however, remains to be explored. We hope that the experimental benchmarks and phenomenological framework provided may stimulate renewed efforts to extend the detailed theoretical modeling of strong-field induced nanoplasma dynamics toward larger systems and longer timescales, ultimately bridging the gap between the few-atom limit and macroscopic plasma phenomena.

Acknowledgments

This research was supported by the U.S. Department of Energy (DOE), Office of Science, Office of Basic Energy Sciences (BES), Chemical Sciences, Geosciences and Biosciences Division, through Contract No. DE-AC02-05CH11231 (C.Ba., A.S.C., C.D.P., D.M.N., O.G.), and Contract No. DE-AC02-06CH11357 (M.B., C.Bo.). A.F.V. was supported by NSF Grants No. DMR-1701077 and DMR-1501276. F.L. acknowledges support by the Austrian Science Fund (FWF, Erwin Schrödinger Fellowship Grant No. J 3580-N20). T.G. acknowledges support by the P. Ewald fellowship of the Volkswagen Foundation and the Panofsky fellowship of SLAC National Accelerator Laboratory. Portions of this research were carried out at the LCLS, a national user facility operated by Stanford University on behalf of the U.S. DOE, Office of Science, Office of BES under beam-time Grant No. LJ54. Use of the Linac Coherent Light Source (LCLS), SLAC National Accelerator Laboratory, is supported by the U.S. DOE, Office of Science, Office of BES under Contract No. DE-AC02-76SF00515. The authors would like to thank Thomas Fennel and Christian Peltz for helpful advice during the early stages of the image analysis.

Author Contributions

O.G., A.F.V. and C.Bo. conceived the experiment, C.Ba., A.S.C, F.L., C.D.P., R.M.P.T., C.Be., D.V., S.O'C., M.B., K.R.F., T.G., R.N.C., G.C., D.R., T.O., C.Bo., A.F.V. and O.G. carried out the experiment. C.Ba., A.S.C, C.Be., A.F.V. and O.G. performed the data analysis and theoretical modeling. C.Ba., A.S.C, F.L., R.M.P.T., T.G., G.C., D.M.N., C.Bo., A.F.V. and O.G wrote the manuscript.

Competing Interests

The authors declare no competing financial interests.

Data Availability Statement

Raw data were generated at the Linac Coherent Light Source (LCLS) large-scale facility. Derived data supporting the findings of this study are available from the corresponding author upon request.

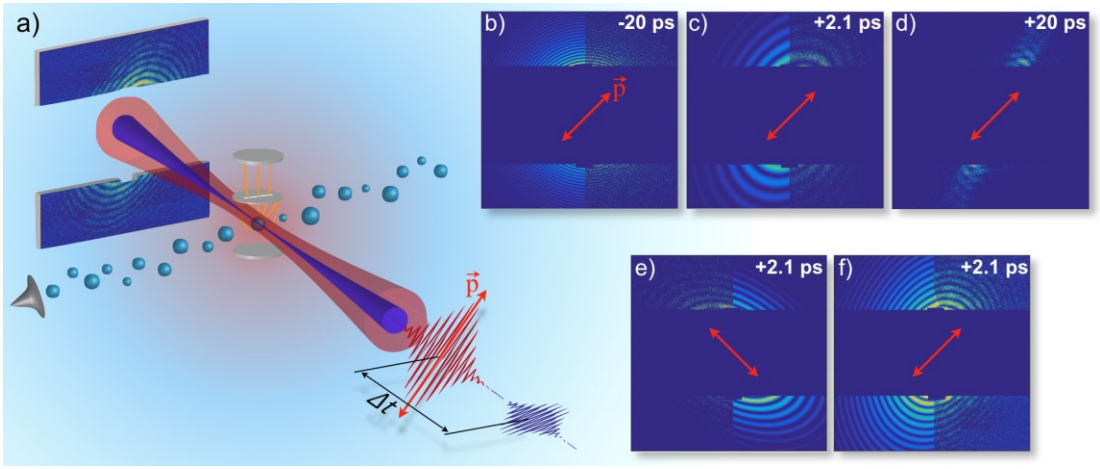

Figure 1: a) Nanoplasmas are generated by exposing helium nanodroplets to an intense, linearly polarized NIR pulse (red). The temporal evolution of the plasmas is probed via coherent X-ray scattering using a delayed X-ray pulse (blue). b-d) Representative scattering patterns for three pump-probe time delays Δt of -20 ps (b), 2.1 ps (c), and 20 ps (d) at a constant NIR polarization (red arrows). e,f) Patterns recorded with two different NIR polarizations at a pump-probe delay of Δt=2.1 ps. In each panel, the scattered points in two of the four quadrants are experimental data, whereas the smooth lines in the other two quadrants are fits as described in the text.

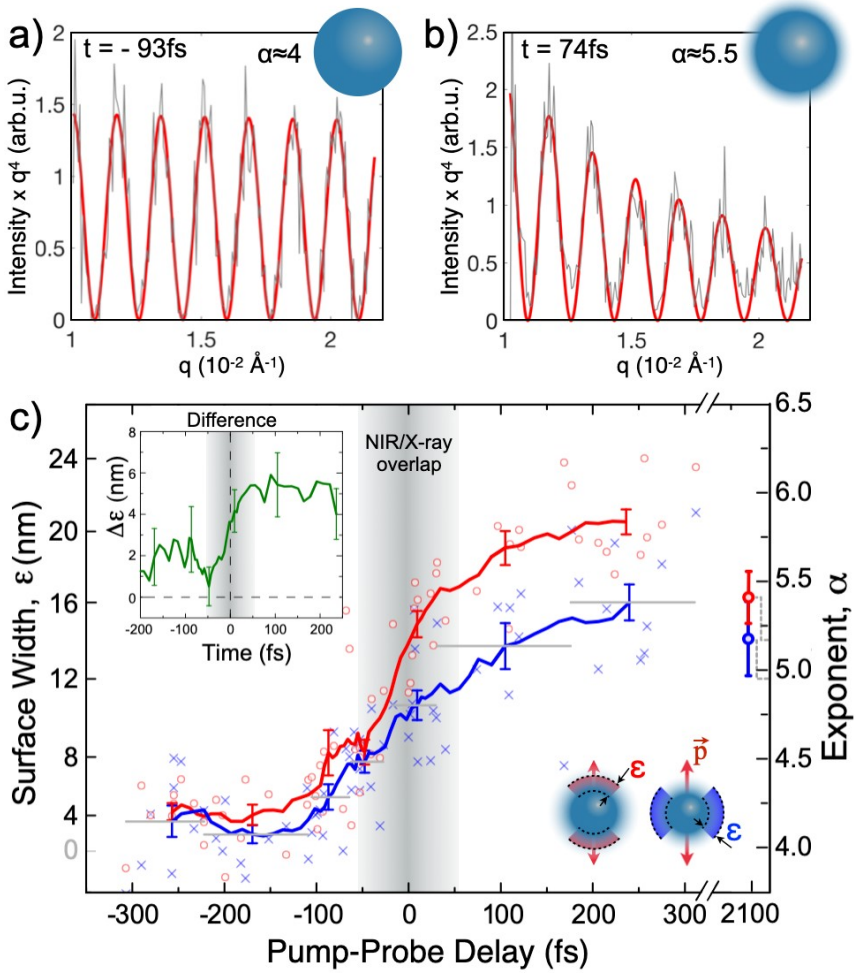

Figure 2: a), b) Power-law fits (red) of azimuthally integrated scattering patterns (gray), indicating exponents of a) $\alpha \approx 4$ and b) $\alpha \approx 5.5$ before and after the NIR laser interacts with the droplet, respectively. Signal intensities are scaled by q^4 for improved clarity. c) Temporal evolution of the exponents α (right) and corresponding 90 % – 10 % surface width ε (left) for 90º wide angular ranges parallel (red) and perpendicular (blue) to the NIR polarization axis. Circles and crosses mark individual data points obtained from single helium droplets, lines represent moving averages integrated over ten data points. Note that the exponent values on the right ordinate apply to all data points except those at 2.1 ps delay, whose values are indicated by the dotted gray lines. The left ordinate applies to all data points. Exemplary vertical error bars indicate uncertainties of the mean values, corresponding horizontal gray lines indicate individual 10-point averaging ranges. The inset shows the average difference between parallel and perpendicular surface widths as deduced from the same images (green). Gray-shaded areas indicate the nominal NIR/X-ray pulse overlap region.

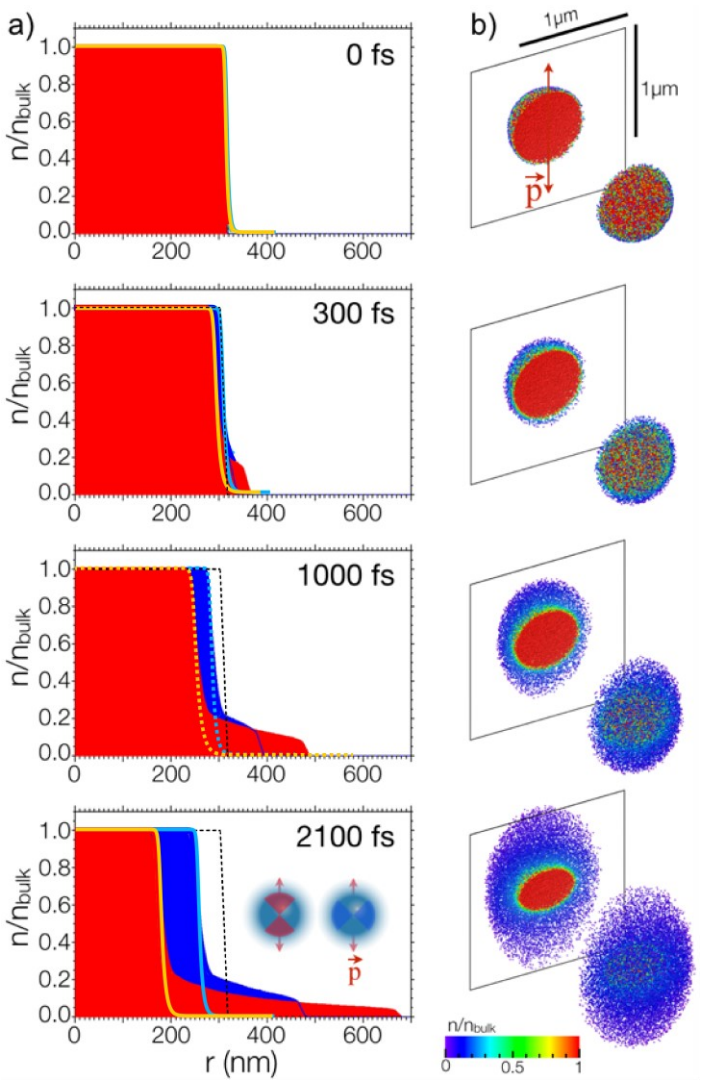

Figure 3: a) Plasma electron density profiles parallel (red) and perpendicular (blue) to the NIR polarization as a function of pump-probe delay. Solid orange and light blue lines are determined experimentally, shaded areas are the result of an anisotropic expansion model. The dashed lines at 1000 fs delay are interpolations of experimental data at delays of 300 fs and 2100 fs. The dotted black lines in the lower three panels indicate the original density profile. The inset in the bottom panel indicates the angular integration ranges for the experimental data. b) Simulated 3D nanoplasma density evolution. Densities are represented by the density of points as well as their colors according to the color bar. The 3D patterns are cut in half in the indicated plane and the front halves are offset to reveal the radial density profiles.

References

[1] T. Ditmire, T. Donnelly, A. M. Rubenchik, R. W. Falcone, and M. D. Perry, Interaction of intense laser pulses with atomic clusters, Phys. Rev. A **53**, 3379 (1996).

[2] T. Ditmire, J. W. G. Tisch, E. Springate, M. B. Mason, N. Hay, J. P. Marangos, and M. H. R. Hutchinson, High Energy Ion Explosion of Atomic Clusters: Transition from Molecular to Plasma Behavior, Phys. Rev. Lett. **78**, 2732 (1997).

[3] M. Lezius, S. Dobosz, D. Normand, and M. Schmidt, Explosion Dynamics of Rare Gas Clusters in Strong Laser Fields, Phys. Rev. Lett. **80**, 261 (1998).

[4] U. Saalmann, C. Siedschlag, and J. M. Rost, Mechanisms of cluster ionization in strong laser pulses, J. Phys. B: At., Mol. Opt. Phys. **39**, R39 (2006).

[5] T. Fennel, K. H. Meiwes-Broer, J. Tiggesbäumker, P. G. Reinhard, P. M. Dinh, and E. Suraud, Laser-driven nonlinear cluster dynamics, Rev. Mod. Phys. **82**, 1793 (2010).

[6] K. Ostrikov, F. Beg, and A. Ng, Colloquium: Nanoplasmas generated by intense radiation, Rev. Mod. Phys. **88**, 011001 (2016).

[7] B. Schütte, M. Arbeiter, A. Mermillod-Blondin, M. J. J. Vrakking, A. Rouzée, and T. Fennel, Ionization Avalanching in Clusters Ignited by Extreme-Ultraviolet Driven Seed Electrons, Phys. Rev. Lett. **116**, 033001 (2016).

[8] M. Kelbg, M. Zabel, B. Krebs, L. Kazak, K. H. Meiwes-Broer, and J. Tiggesbäumker, Temporal Development of a Laser-Induced Helium Nanoplasma Measured through Auger Emission and Above-Threshold Ionization, Phys. Rev. Lett. **125**, 093202 (2020).

[9] T. Döppner, T. Diederich, A. Przystawik, N. X. Truong, T. Fennel, J. Tiggesbäumker, and K. H. Meiwes-Broer, Charging of metal clusters in helium droplets exposed to intense femtosecond laser pulses, Phys. Chem. Chem. Phys. **9**, 4639 (2007).

[10] C. Bostedt, H. Thomas, M. Hoener, E. Eremina, T. Fennel, K. H. Meiwes-Broer, H. Wabnitz, M. Kuhlmann, E. Plönjes, K. Tiedtke *et al.*, Multistep Ionization of Argon Clusters in Intense Femtosecond Extreme Ultraviolet Pulses, Phys. Rev. Lett. **100**, 133401 (2008).

[11] B. F. Murphy, K. Hoffmann, A. Belolipetski, J. Keto, and T. Ditmire, Explosion of Xenon Clusters Driven by Intense Femtosecond Pulses of Extreme Ultraviolet Light, Phys. Rev. Lett. **101**, 203401 (2008).

[12] S. R. Krishnan, C. Peltz, L. Fechner, V. Sharma, M. Kremer, B. Fischer, N. Camus, T. Pfeifer, J. Jha, M. Krishnamurthy *et al.*, Evolution of dopant-induced helium nanoplasmas, New J. Phys. **14**, 075016 (2012).

[13] L. F. Gomez, K. R. Ferguson, J. P. Cryan, C. Bacellar, R. M. P. Tanyag, C. Jones, S. Schorb, D. Anielski, A. Belkacem, C. Bernando *et al.*, Shapes and Vorticities of Superfluid Helium Nanodroplets, Science **345**, 906 (2014).

[14] T. Gorkhover, S. Schorb, R. Coffee, M. Adolph, L. Foucar, D. Rupp, A. Aquila, J. D. Bozek, S. W. Epp, B. Erk *et al.*, Femtosecond and nanometre visualization of structural dynamics in superheated nanoparticles, Nat. Photonics **10**, 93 (2016).

[15] L. Flückiger, D. Rupp, M. Adolph, T. Gorkhover, M. Krikunova, M. Müller, T. Oelze, Y. Ovcharenko, M. Sauppe, S. Schorb *et al.*, Time-resolved x-ray imaging of

a laser-induced nanoplasma and its neutral residuals, New J. Phys. **18**, 043017 (2016).

[16] C. Bostedt, E. Eremina, D. Rupp, M. Adolph, H. Thomas, M. Hoener, A. R. B. de Castro, J. Tiggesbäumker, K. H. Meiwes-Broer, T. Laarmann *et al.*, Ultrafast X-Ray Scattering of Xenon Nanoparticles: Imaging Transient States of Matter, Phys. Rev. Lett. **108**, 093401 (2012).

[17] B. Langbehn, K. Sander, Y. Ovcharenko, C. Peltz, A. Clark, M. Coreno, R. Cucini, M. Drabbels, P. Finetti, M. Di Fraia *et al.*, Three-Dimensional Shapes of Spinning Helium Nanodroplets, Phys. Rev. Lett. **121**, 255301 (2018).

[18] S. M. O. O'Connell, R. M. P. Tanyag, D. Verma, C. Bernando, W. Pang, C. Bacellar, C. A. Saladrigas, J. Mahl, B. W. Toulson, Y. Kumagai *et al.*, Angular Momentum in Rotating Superfluid Droplets, Phys. Rev. Lett. **124**, 215301 (2020).

[19] D. Rupp, L. Flückiger, M. Adolph, A. Colombo, T. Gorkhover, M. Harmand, M. Krikunova, J. P. Müller, T. Oelze, Y. Ovcharenko *et al.*, Imaging plasma formation in isolated nanoparticles with ultrafast resonant scattering, Struct. Dyn. **7**, 034303 (2020).

[20] T. Nishiyama, Y. Kumagai, A. Niozu, H. Fukuzawa, K. Motomura, M. Bucher, Y. Ito, T. Takanashi, K. Asa, Y. Sato *et al.*, Ultrafast Structural Dynamics of Nanoparticles in Intense Laser Fields, Phys. Rev. Lett. **123**, 123201 (2019).

[21] C. Peltz, C. Varin, T. Brabec, and T. Fennel, Time-Resolved X-Ray Imaging of Anisotropic Nanoplasma Expansion, Phys. Rev. Lett. **113**, 133401 (2014).

[22] V. Kumarappan, M. Krishnamurthy, and D. Mathur, Two-dimensional effects in the hydrodynamic expansion of xenon clusters under intense laser irradiation, Phys. Rev. A **66**, 033203 (2002).

[23] D. R. Symes, M. Hohenberger, A. Henig, and T. Ditmire, Anisotropic Explosions of Hydrogen Clusters under Intense Femtosecond Laser Irradiation, Phys. Rev. Lett. **98**, 123401 (2007).

[24] E. Springate, N. Hay, J. W. G. Tisch, M. B. Mason, T. Ditmire, M. H. R. Hutchinson, and J. P. Marangos, Explosion of atomic clusters irradiated by high-intensity laser pulses: Scaling of ion energies with cluster and laser parameters, Phys. Rev. A **61**, 063201 (2000).

[25] V. Kumarappan, M. Krishnamurthy, and D. Mathur, Asymmetric High-Energy Ion Emission from Argon Clusters in Intense Laser Fields, Phys. Rev. Lett. **87**, 085005 (2001).

[26] M. Krishnamurthy, D. Mathur, and V. Kumarappan, Anisotropic "charge-flipping" acceleration of highly charged ions from clusters in strong optical fields, Phys. Rev. A **69**, 033202 (2004).

[27] M. Hirokane, S. Shimizu, M. Hashida, S. Okada, S. Okihara, F. Sato, T. Iida, and S. Sakabe, Energy distributions of ions emitted from argon clusters Coulomb-exploded by intense femtosecond laser pulses, Phys. Rev. A **69**, 063201 (2004).

[28] E. Skopalovà, Y. C. El-Taha, A. Zaïr, M. Hohenberger, E. Springate, J. W. G. Tisch, R. A. Smith, and J. P. Marangos, Pulse-Length Dependence of the Anisotropy of Laser-Driven Cluster Explosions: Transition to the Impulsive Regime for Pulses Approaching the Few-Cycle Limit, Phys. Rev. Lett. **104**, 203401 (2010).

[29] D. Mathur, F. A. Rajgara, A. R. Holkundkar, and N. K. Gupta, Strong-field ionization and Coulomb explosion of argon clusters by few-cycle laser pulses, Phys. Rev. A **82**, 025201 (2010).

[30] A. Mikaberidze, U. Saalmann, and J. M. Rost, Laser-Driven Nanoplasmas in Doped Helium Droplets: Local Ignition and Anisotropic Growth, Phys. Rev. Lett. **102**, 128102 (2009).

[31] K. R. Ferguson, M. Bucher, J. D. Bozek, S. Carron, J.-C. Castagna, R. Coffee, G. I. Curiel, M. Holmes, J. Krzywinski, M. Messerschmidt *et al.*, The Atomic, Molecular and Optical Science instrument at the Linac Coherent Light Source, J. Synchrotron Radiat. **22**, 492 (2015).

[32] H. Buchenau, E. L. Knuth, J. Northby, J. P. Toennies, and C. Winkler, Mass spectra and time-of-flight distributions of helium cluster beams, J. Chem. Phys. **92**, 6875 (1990).

[33] B. Walker, B. Sheehy, L. F. DiMauro, P. Agostini, K. J. Schafer, and K. C. Kulander, Precision Measurement of Strong Field Double Ionization of Helium, Phys. Rev. Lett. **73**, 1227 (1994).

[34] C. Bacellar, A. S. Chatterley, F. Lackner, C. D. Pemmaraju, R. M. P. Tanyag, D. Verma, C. Bernando, S. O'Connell, M. Bucher, K. R. Ferguson *et al.*, Anisotropic surface broadening and core depletion during the evolution of a strong-field induced nanoplasma - Supplemental Material, Phys. Rev. Lett. ***submitted***.

[35] C. Bernando, R. M. P. Tanyag, C. Jones, C. Bacellar, M. Bucher, K. R. Ferguson, D. Rupp, M. Ziemkiewicz, L. F. Gomez, A. S. Chatterley *et al.*, Shapes of rotating superfluid helium nanodroplets, Phys. Rev. B **95**, 064510 (2017).

[36] T. Pfeifer, C. Spielmann, and G. Gerber, Femtosecond x-ray science, Rep. Prog. Phys. **69**, 443 (2006).

[37] D. Verma, S. M. O. O'Connell, A. J. Feinberg, S. Erukala, R. M. P. Tanyag, C. Bernando, W. Pang, C. A. Saladrigas, B. W. Toulson, M. Borgwardt *et al.*, Shapes of rotating normal fluid 3He versus superfluid 4He droplets in molecular beams, Phys. Rev. B **102**, 014504 (2020).

[38] R. M. P. Tanyag, C. Bernando, C. F. Jones, C. Bacellar, K. R. Ferguson, D. Anielski, R. Boll, S. Carron, J. P. Cryan, L. Englert *et al.*, Communication: X-ray coherent diffractive imaging by immersion in nanodroplets, Struct. Dyn. **2**, 051102 (2015).

[39] A. J. Feinberg, D. Verma, S. M. O. O'Connell-Lopez, S. Erukala, R. M. P. Tanyag, W. Pang, C. A. Saladrigas, B. W. Toulson, M. Borgwardt, N. Shivaram *et al.*, Aggregation of solutes in bosonic versus fermionic quantum fluids, Science Advances **7**, eabk2247 (2021).

[40] M. Hoener, C. Bostedt, H. Thomas, L. Landt, E. Eremina, H. Wabnitz, T. Laarmann, R. Treusch, A. R. B. d. Castro, and T. Möller, Charge recombination in soft x-ray laser produced nanoplasmas, J. Phys. B: At., Mol. Opt. Phys. **41**, 181001 (2008).

[41] D. Rupp, L. Flückiger, M. Adolph, T. Gorkhover, M. Krikunova, J. P. Müller, M. Müller, T. Oelze, Y. Ovcharenko, B. Röben *et al.*, Recombination-Enhanced Surface Expansion of Clusters in Intense Soft X-Ray Laser Pulses, Phys. Rev. Lett. **117**, 153401 (2016).

[42] T. V. Liseykina and D. Bauer, Plasma-Formation Dynamics in Intense Laser-Droplet Interaction, Phys. Rev. Lett. **110**, 145003 (2013).